Journal of Materials Processing Technology 214 (2014) 477–484

Contents lists available at ScienceDirect

Journal of Materials Processing Technology

journal homepage: www.elsevier.com/locate/jmatprotec

Dissimilar joining of AA2024 aluminum studs and AZ80 magnesium plates by high-speed solid-state welding

Yohei Harada[a,*], Yutaro Sada[b], Shinji Kumai[c]

[a] Department of Materials Science and Engineering, Interdisciplinary Graduate School of Science and Engineering, Tokyo Institute of Technology, 4259 Nagatsuta-cho Midori-ku, Yokohama, Kanagawa 226-8502, Japan
[b] Tokyo Institute of Technology, 4259 Nagatsuta-cho Midori-ku, Yokohama, Kanagawa 226-8502, Japan
[c] Department of Metallurgy and Ceramics Science, Graduate School of Science and Engineering, Tokyo Institute of Technology, 2-12-1 Ookayama Meguro-ku, Tokyo 152-8552, Japan

ARTICLE INFO

Article history:
Received 30 May 2013
Received in revised form 8 October 2013
Accepted 10 October 2013
Available online 19 October 2013

Keywords:
Dissimilar joining
Aluminum alloy stud
Magnesium alloy plate
High-speed solid-state welding
Intermetallics

ABSTRACT

An AA2024 aluminum stud having a circular projection at its bottom was pressed against AZ80 magnesium plate, whereupon a discharge current applied to the upper part of the stud flowed through the point of contact between the projection and the plate to form a joint between them. The effects of discharge voltage on the joint tensile fracture load and the interfacial microstructure were evaluated. The fracture load increased with discharge voltage up to 300 V but decreased gradually thereafter. Observations of joint areas revealed a structure in which the projection penetrated into the plate and was bent toward the outer side, in line with the predominant path of current flow. Refined grains of AZ80 magnesium were observed near the joint interface. This suggests that local plastic deformation and heating induced dynamic recrystallization within the plate. A thin intermediate phase layer approximately 1 μm thick was observed along the joint interface. Compositional analysis by Auger electron spectroscopy confirmed the presence of both $Mg_{17}Al_{12}$ and Al_3Mg_2 in the intermediate phase. The very low heat input required in high-speed solid-state welding ensured a very thin intermediate phase layer. This resulted in a defect-free strong joint between the aluminum and magnesium alloys.

1. Introduction

Arc stud welding and resistance spot welding are common stud welding methods that are widely used for joining metallic studs, such as pins or screws, to a metallic plate. These conventional methods generate excess heat input for melting the joint materials during the welding process. Chambers (2001) reported the principles of the stud welding, in which the welding involves the molten metals of both the stud and the plate. Ramasamy (2002) reported that sufficient melting is required for optimal weld integrity in arc stud welding. Distortion of thin plates is shown in that report. In the case of thin plates and surface-treated or painted plates, distortion of the plate and tarnishing of the back surface of the plate become serious problems. A high-speed solid-state welding has recently been developed to resolve these problems. In this method, joining is completed within a few milliseconds by using a large discharge current and pressure. The stud is specially designed to have a circular projection at the bottom. The stud shape, electrode shape, and current path are controlled in this method to obtain a sound joint while suppressing excess heat input. One feature of this method is that, unlike conventional methods, it does not distort thin plate or tarnish its back surface. Kumai et al. (2011) previously reported on the applicability of this method to joining AA2024-T3 aluminum studs to AA5052-H34 aluminum plate. The stud and plate are strongly joined without the back surface of the plate becoming tarnished. With the exception of the tip, the projection is severely deformed and spreads along the plate surface, with joining achieved in this area. No joint forms at the projection tip that penetrated into the plate before the discharge voltage was applied. Takaya et al. (2012) also reported the joining of AA2024-T3 aluminum studs to AA6N01-T6 aluminum plate. A softened zone appears at the plate adjacent to the joint interface. The hardness of the softened zone recovers to that of AA6N01 aluminum upon post-joint aging. That finding indicates that softening is caused by the dissolution of β'' precipitates in the aluminum matrix due to the welding heat input. Kumai and Takaya (2012) clarified the effects of plate thickness on interfacial microstructure and joint strength. In the case of thick plates (e.g., 3 and 4 mm), the projection deforms almost symmetrically and joining is achieved on both sides of the projection, resulting in high joint strength. In contrast, the deformation of the thin plate (e.g., 1 mm) is asymmetric between the outer and inner sides of the projection. The joining is achieved at mainly the outer side of

* Corresponding author. Tel.: +81 45 924 5620.
E-mail address: harada.y.ah@m.titech.ac.jp (Y. Harada).

0924-0136/$ – see front matter © 2013 Elsevier B.V. All rights reserved.
http://dx.doi.org/10.1016/j.jmatprotec.2013.10.005

Table 1
Chemical compositions of materials used in this study, mass%.

Cu	Mg	Mn	Si	Fe	Cr	Zn	Ti	Al
(a) AA2024 aluminum stud								
<3.8–4.9	1.2–1.8	0.30–0.90	<0.50	<0.50	<0.10	<0.25	<0.15	Bal.

Al	Zn	Mn	Fe	Si	Cu	Ni	Mg
(b) AZ80 magnesium extruded plate							
8.20	0.59	0.18	0.0008	0.0078	0.0006	0.0005	Bal.

the projection, decreasing the joint strength. Kumai and Hayashida (2012) also attempted to modify the shape of the projection in order to improve the joining strength of the joints. When a stud whose projection tip is shifted toward the inner side is used, the projection spreads much wider along the plate surface on the outer side than the inner side. This effectively acts to increase the joint area on the outer side and the resultant joining strength. This demonstrates that modifying the shape of the projection is useful for stud welding on thin plate.

Recently, magnesium alloys have received considerable attention due to their many attractive characteristics, such as low density, high electromagnetic shielding, high damping capacity, and good machinability. Schubert et al. (2001) argued that Al–Mg joints are an optimal material for future applications in the automotive and aerospace industries. The present study focuses on the dissimilar joining of aluminum alloys to magnesium alloys. An important problem in dissimilar joining is the formation of brittle intermetallic compounds consisting of aluminum and magnesium. For instance, Watanabe and Sugiyama (2004) have reported that thick layers of brittle intermetallic compound decrease the strength of joints formed at the interface between 1050 commercially pure aluminum plate and AZ31 magnesium plate when conventional resistance spot welding is used. Firouzdor and Kou (2010) reported the effect of welding conditions on heat input and joint strength in friction stir welded AA6061/AZ31 joints. The welding conditions have a significant effect on heat input, which in turn has a significant effect on the formation of brittle intermetallic compounds and even liquid films. The liquid films cause cracking during stirring and formation of intermetallic compounds upon solidification. Both cracking and intermetallic compounds in the stir zone lower the joint strength. Heat input is a key variable governing the effects of the welding conditions on joint strength. Bhamji et al. (2012) reported the effects of welding parameters on intermetallic phase fractions in linear friction welded AA6082/AZ31 joints: even small weight fractions of the intermetallic phase compromise the mechanical properties. Reducing the heat input for joining is therefore necessary for suppressing the formation of excess intermetallic compounds. High-speed solid-state welding is one candidate for accomplishing sound joints of aluminum alloy studs to magnesium alloy plate.

In the present study, the applicability of the high-speed solid-state welding to the dissimilar joining of high strength AA2024 aluminum studs to AZ80 magnesium extruded plate was examined. The effect of joining parameters on the interfacial microstructure and the joint tensile fracture load were also investigated.

2. Experimental procedures

2.1. Materials

Materials used in this study were specially designed AA2024-T3 aluminum studs and AZ80-F magnesium extruded plate (thickness: 3 mm). The chemical compositions of the materials are listed in Table 1. Fig. 1(a) and (b) shows a photograph and cross-sectional

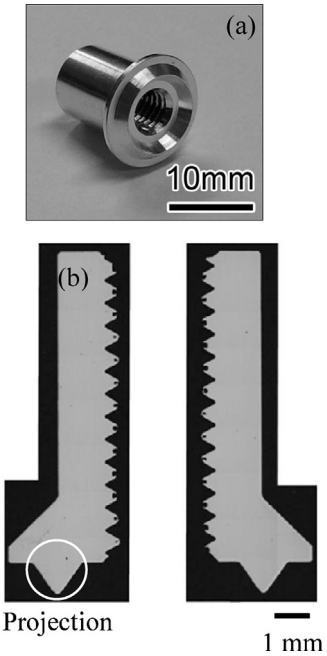

Fig. 1. (a) Photograph and (b) cross-sectional view of a stud.

view of a stud. The stud has a circular projection at the bottom. The projection height is 1 mm and the projection tip diameter is 7 mm.

2.2. Joining principle

Fig. 2(I)–(IV) illustrates the joining sequence. Two concentric cylindrical copper tubes are utilized, with the inner and outer tubes arranged to complete a discharge circuit. (I) A stud is mounted onto the end of the inner tube. (II) The stud and the outer tube are pressed against a plate surface by air pressure. (III) A discharge current is introduced to the stud through the inner tube. The current flows through the plate surface to the outer tube, which serves as ground. Local heating can be achieved by the controlled current route with the high current density at the contact point between the projection and plate. The projection and plate are deformed by local heating and pressure. (IV) The air pressure is released after the current flow is stopped. Since the deformed projection and plate make contact at a bare surface newly formed by the removal of the oxide film, joining can be achieved at the contact point.

2.3. Joining conditions

Joining experiments were performed with a stud-welding machine developed by Akebono Kikai Ltd. The joining parameters are shown in Table 2. Discharge voltages of 250–400 V were utilized. Other parameters, such as the air pressure for loading the stud (0.45 MPa) and discharge capacitor capacitance (67,500 μF × 6 banks) were kept constant.

2.4. Microstructural analysis

Joint specimens were cut in half, perpendicular to the joint interface. The cross sections were ground with waterproof

Table 2
Joining parameters.

Discharge voltage	Air pressure	Discharge capacitor capacitance
250, 300, 350, 400 V	0.45 MPa	67,500 μF – 6 banks

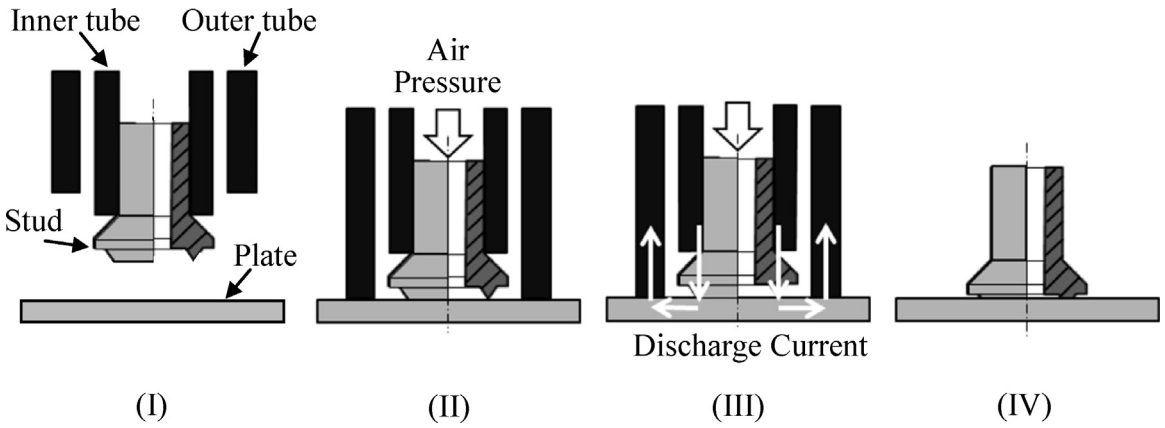

Fig. 2. Schematic illustration of joining sequence.

abrasive paper sheets up to #4000 and then polished with diamond paste (3 μm, 1 μm). The polished surfaces were etched in a solution of 10 g picric acid, 200 mL ethanol, 10 mL acetic acid, and 20 mL distilled water in order to observe the grain structure of the AZ80 magnesium plate. The microstructures of the joint interfaces were observed by optical microscopy (OM) and back-scattered electron imaging (BEI) using a scanning electron microscope (SEM). Compositional analysis of the interfacial microstructure was carried out using an electron probe micro analyzer (EPMA) fitted to an SEM and using Auger electron spectroscopy (AES) on a field-emission SEM (FE-SEM).

2.5. Mechanical test

Vickers hardness measurement under an indenter load of 50 gf was carried out. To investigate the tensile fracture load, joint specimens were loaded in tension perpendicular to the joint interface. Fig. 3 shows a schematic diagram of the tensile test. Crosshead speed was kept constant at 0.1 mm/min. Fracture surfaces were observed by secondary electron imaging (SEI) using an SEM.

3. Results and discussion

3.1. Joint tensile fracture load and interfacial microstructure

Fig. 4 shows the relationship between tensile fracture load and discharge voltage. In the present study, the deformation behavior of the projection and the joining area varied with discharge voltage. Joint strength was evaluated by using the tensile fracture load, because it was difficult to measure the joining area accurately after the tensile fracture test. The fracture load increased with discharge voltage up to 300 V, but decreased gradually thereafter. It was important to select an appropriate discharge voltage in order to obtain maximum fracture load. The tensile fracture load of the joints was expected to be strongly related to the interfacial microstructure.

Cross-sectional images of the stud before joining and after joining are shown in Fig. 5. The deformed projection was observed after joining. Fig. 6(a)–(e) shows magnified optical micrographs of the framed part in Fig. 5, (a) after only pressing the stud without applying the discharge voltage, and after joining under discharge voltages of (b) 250 V, (c) 300 V, (d) 350 V, and (e) 400 V. Left and

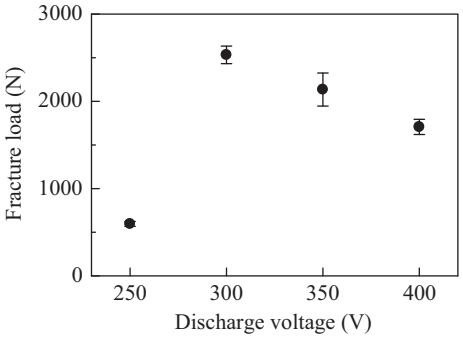

Fig. 4. Relationship between tensile fracture load and discharge voltage.

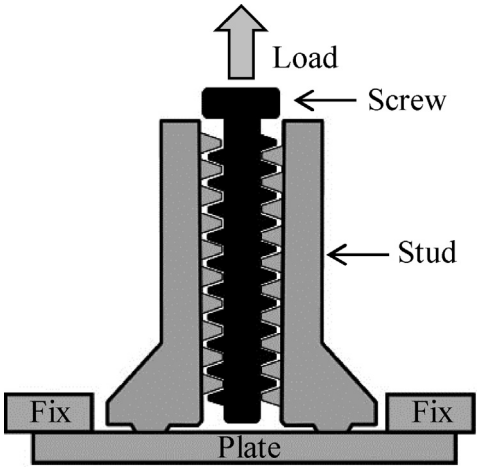

Fig. 3. Schematic diagram of tensile test.

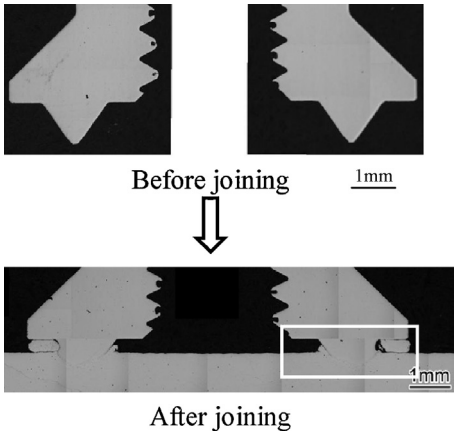

Fig. 5. Cross-sectional images of a stud before and after joining.

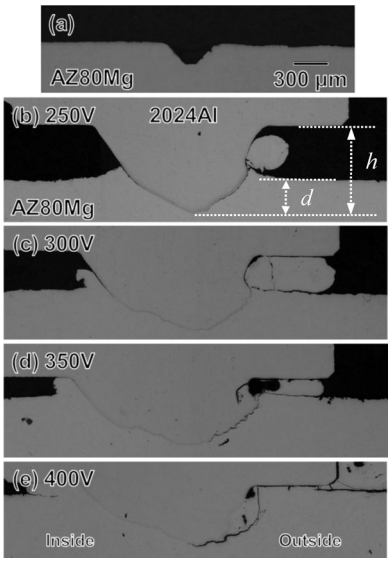

Fig. 6. Optical micrographs of framed area in Fig. 5, (a) after only stud pressing without applying discharge voltage, and after joining under discharge voltages of (b) 250 V, (c) 300 V, (d) 350 V, and (e) 400 V.

right in the figures correspond to inner and outer sides of the projection, respectively. In Fig. 6(a), the depth of the stub indentation is about 200 μm. Since no discharge voltage was applied, no joining was achieved in this case. In the case of joining under discharge voltages of 250–400 V, observation of the joint area revealed that the AA2024 aluminum projection penetrated into the AZ80 magnesium plate. As the discharge voltage increased, the projection bent toward the outer side of the stud, in line with the predominant current route. This deformation behavior is notably different from that in previous reports on joining AA2024 aluminum studs to AA5052 aluminum plate (Kumai et al., 2011) and to AA6N01 aluminum plate (Takaya et al., 2012). In those cases, the majority of the projection became severely deformed and spread along the plate surface with the exception of the projection tip, which penetrated into the plate before the discharge voltage was applied. Since the electrical conductivity, heat conductivity, and solidus temperature of AZ80 magnesium are lower than those of AA2024 aluminum, the plate (AZ80) softens preferentially allowing the projection (AA2024) to penetrate into it. Furthermore, the projection tended to deform more severely with increasing discharge voltage, as shown in Fig. 6. Here, h is defined as the height between the projection base and the projection tip, and d as the penetration depth of the projection tip into the plate surface. Fig. 7 shows how the projection height h and sticking depth d varied with discharge voltage. As the discharge voltage increased, the projection height decreased while the sticking depth increased. Joule heating is thought to produce local

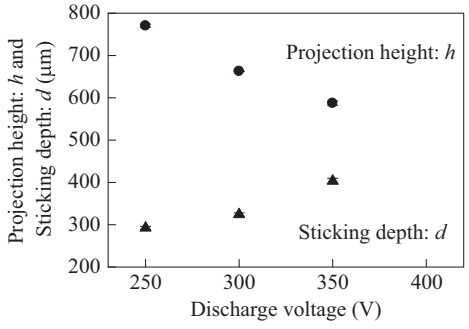

Fig. 7. Variation of projection height h and sticking depth d with discharge voltage.

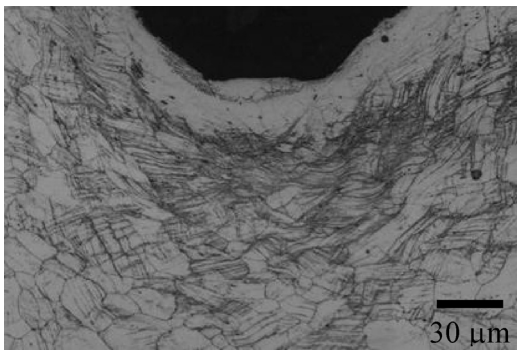

Fig. 8. Cross-sectional image of etched AZ80 magnesium plate near the stub indentation after stud pressing.

heating sufficient to soften both the AA2024 aluminum and AZ80 magnesium at the joint interface. Cracking was observed toward the outer side of the projection under high discharge voltages. The extent of cracking increased with increasing discharge voltage. At 250 V, sufficient joining was not achieved except around the projection tip, with a gap observed between the projection and the plate on both sides of the projection. At 300 V, however, joining was achieved on both sides of the projection, increasing the joining area. At 350 V and higher, cracks formed on the outer side of the projection, decreasing the joining area. In the present results, the fracture load was strongly related to the joining area.

Fig. 8 shows across-sectional magnified image of etched AZ80 magnesium plate near the stub indentation shown in Fig. 6(a) after stud pressing. Many deformation twins, which commonly form during the plastic deformation of magnesium, were observed beneath the indentation.

Fig. 9(a)–(c) shows optical micrographs of etched cross sections of joint interfaces formed under a discharge voltage of 250 V. Secondary particles originally existing within the AA2024 aluminum stud were observed. Part of the plate was extruded by the projection toward the outer side of the plate surface, as shown in (a). Magnified images of the framed areas in (a) are shown in (b) and (c). Refined grains of AZ80 magnesium were observed near the interface. The refined grains were several micrometers in size. These grains were much finer than the original grains of the magnesium alloy plate before joining (Fig. 10). The existence of these fine grains reveals dynamic recrystallization of the plate upon local plastic deformation and heating. A thin intermediate phase layer (indicated by arrows) was also observed along part of the outer side of the joint interface (Fig. 9(b)). On the inner side of the joint interface (Fig. 9(c)), although refined grains of AZ80 magnesium were observed near the interface, no joining occurred between the projection and the plate; hence the gap. Similarly, no thin intermediate phase layer was observed along the joint interface.

Fig. 11(a) and (b) shows optical micrographs of etched cross sections of the joint interface formed under a discharge voltage of 300 V. Part of the plate was extruded by the projection toward the outer side of the plate surface, as shown in (a). A magnified image of the framed area in (a) is shown in (b). Joining was also achieved on the inner side of the projection as well as on the outer side. A thin intermediate phase layer was observed along the joint interface. Fig. 11(c) shows a magnified SEM-BEI micrograph of the joint interface. The intermediate phase layer was about 1 μm thick and exhibited different contrast from either the stud or plate. Fig. 12(a) shows a view of the bottom of a stud that had been joined under a discharge voltage of 300 V and then later extracted from the plate by tensile test. The circular projection can be clearly observed. A magnified SEM-SEI micrograph of the framed area in (a) is shown in (b). Several cracks were observed on only the inner side of the

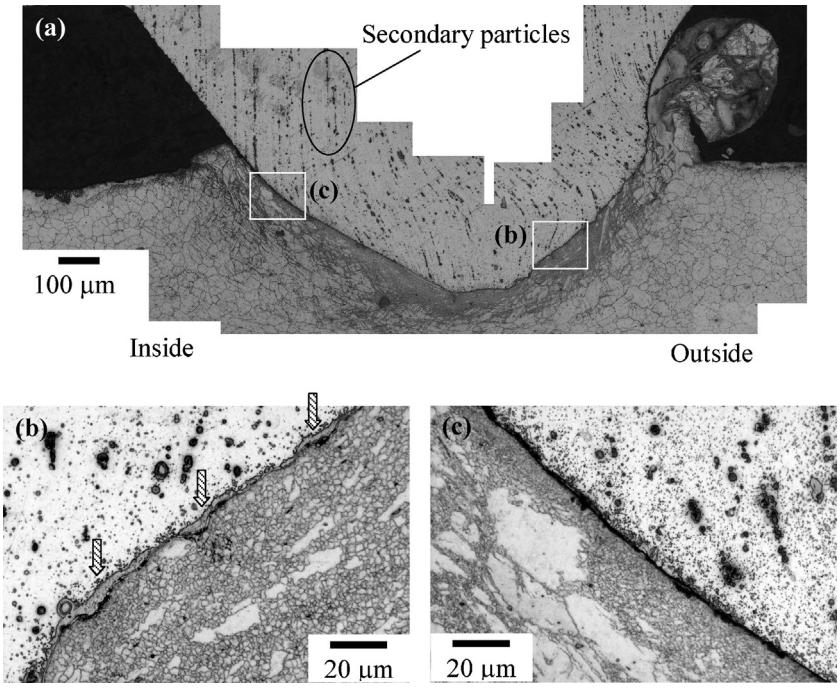

Fig. 9. Optical micrographs of etched cross sections of the joint interface formed under discharge voltage of 250 V. Magnified images of framed areas in (a) are shown in (b) and (c).

projection (indicated by arrow). Such cracks were not observed at 250 V. As shown in Fig. 6(c), at 300 V the projection bent toward the outer side and the inner side of the projection was more severely deformed than in the sample joined at 250 V (Fig. 6(b)). These cracks are therefore thought to occur as the projection deforms toward the outer side. Fig. 13(a) and (b) shows SEM-SEI micrographs of the tensile fracture surface on the plate after the tensile test on the inner side and outer side of the projection indentation, respectively. The fracture surface was covered in both smooth and dimpled structures, indicating ductile fracture. This indicates that the stud and plate were joined strongly enough for the base material to partially fracture during the tensile test. Maximum tensile fracture load was achieved in specimens joined under a discharge voltage of 300 V. The joint interfaces of those specimens were mainly covered with a thin intermediate phase layer. This suggests that a successful joint between the projection and the plate is formed when the interfacial temperature increases sufficiently to form a thin intermediate phase layer. Thus, the most important factor for good joining is optimal temperature around the projection to promote local plastic deformation and atomic diffusion. As shown in Figs. 6 and 7, the projection tended to deform more severely as the discharge voltage was increased. This indicates that the temperature around the projection increases with discharge voltage. If the temperature around the projection is too low because of a low discharge voltage (e.g., 250 V), the resulting joint will be insufficient. The fracture load of the specimens joined under a discharge voltage of 250 V was low because joining was achieved successfully along only part of the outer side of the projection, where a thin intermediate phase layer was partially formed, as shown in Fig. 9(b).

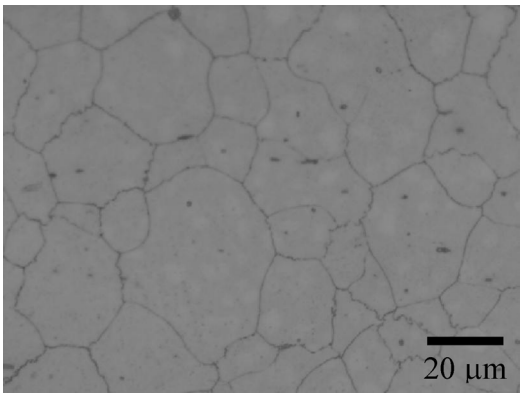

Fig. 10. Original grains of AZ80 magnesium plate before joining.

Fig. 14(a) and (b) shows optical micrographs of etched cross sections of the joint interfaces formed under discharge voltages of 350 and 400 V. The outer sides of the projections were extruded together with the plate toward the outer side of the plate surface, which did not occur at 250 or 300 V. The inner sides of the projections did not become extruded. Only the plate extruded on the inner side of the projections, the same as at 250 and 300 V. This indicates that the outer side of the projection becomes hotter than the inner side because the current predominantly flows between the projection and the plate toward the outer side of the projection. Fig. 15(a) and (b) shows SEM-BEI micrographs of the joint interface that formed under a discharge voltage of 400 V. In Fig. 15(a), a large intermediate phase area (indicated by the arrow) was observed in which the secondary particles that originally existed within the AA2024 aluminum stud had disappeared. Cracks were also observed within the intermediate phase area and along the joint interface between the AA2024 aluminum stud and AZ80 magnesium plate. Vickers hardness was about 200 in this area, which is harder than the AA2024 aluminum stud (Hv: 120) or AZ80 magnesium plate (Hv: 60). Compositional analysis by EPMA found that the intermetallic compound was $Mg_{17}Al_{12}$ phase. This indicates that the temperature increased sufficiently to melt part of both the stud and plate on the outer side of the projection under high discharge voltages, and a thick intermetallic compound area formed and cracked. Firouzdor and Kou (2010) reported on cracking near the intermetallic compound in friction stir welded AA6061/AZ31 joints. They also explained that the liquid films formed by the heat input caused formation of intermetallic compounds and cracking

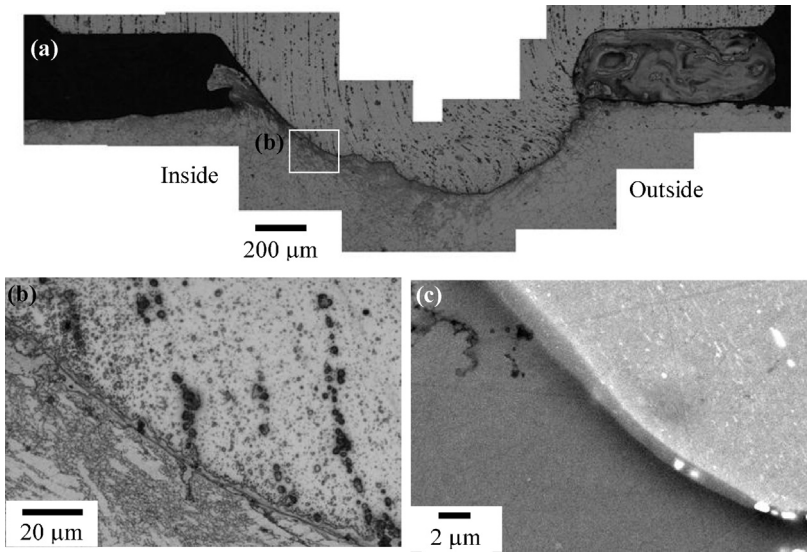

Fig. 11. (a) Optical micrographs of etched cross sections of the joint interface formed under a discharge voltage of 300 V. (b) Magnified image of framed area in (a). (c) Magnified SEM-BEI micrograph of joint interface.

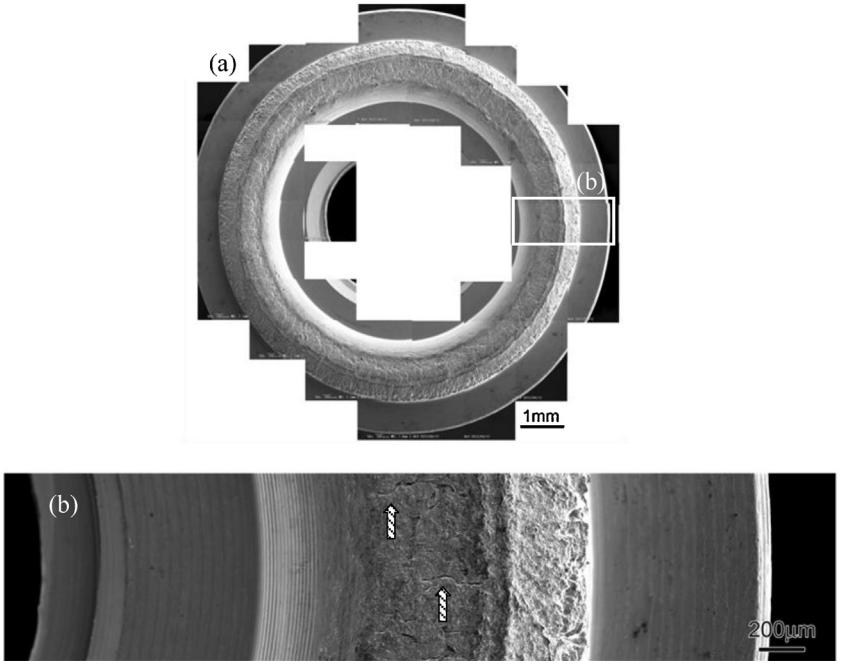

Fig. 12. Bottom of stud extracted from the plate by tensile test. Magnified SEM-SEI micrograph of framed area in (a) is shown in (b).

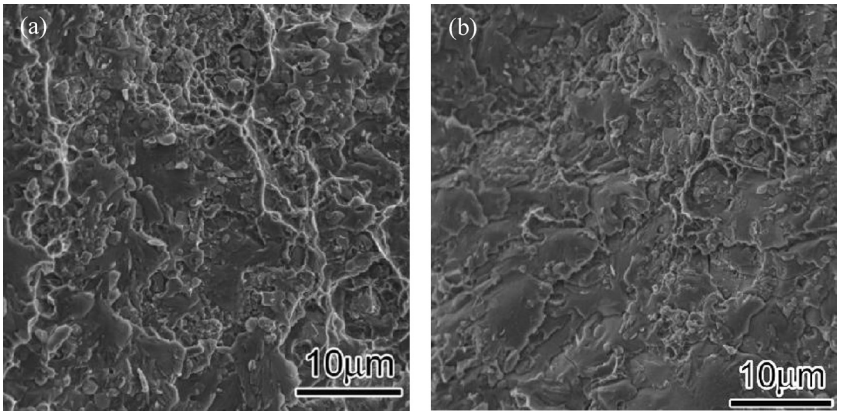

Fig. 13. SEM-SEI micrographs of tensile fracture surface on the plate after the tensile test, corresponding to (a) inner side and (b) outer side of the projection indentation, respectively.

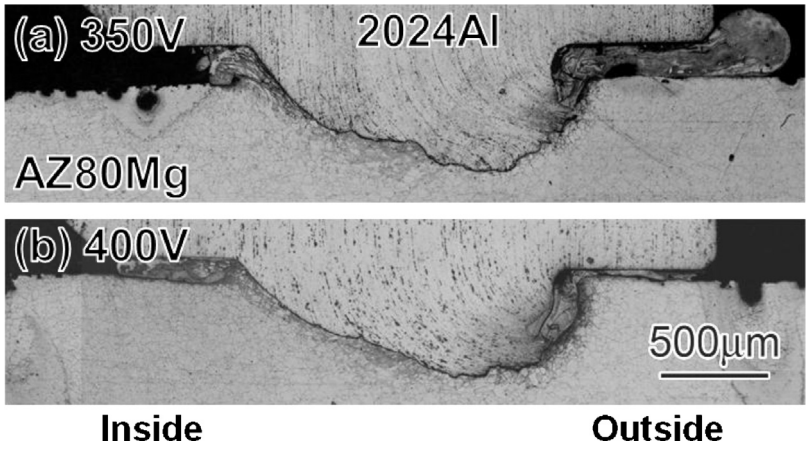

Fig. 14. Optical micrographs of etched cross sections of joint interface formed under discharge voltages of (a) 350 V and (b) 400 V.

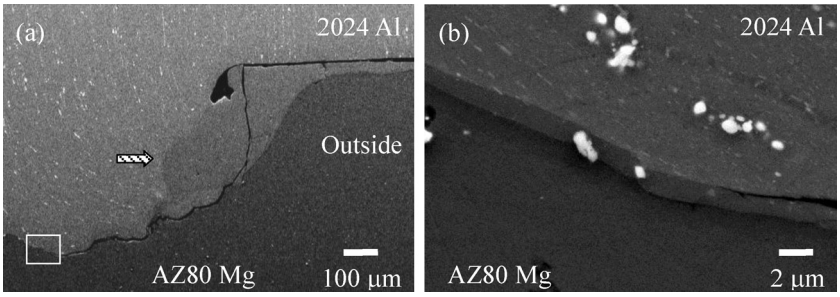

Fig. 15. SEM-BEI micrographs of joint interface formed under discharge voltage of 400 V. (b) Magnified image of joint interface area at the end of a crack (the framed area in (a)).

upon solidification. The reduced fracture load of specimens joined under discharge voltages of 350 and 400 V was caused by a smaller joining area, the same as at 250 V. Fig. 15(b) shows a magnified SEM-BEI micrograph of the part of the joint interface at the end of the crack (the frame area in Fig. 15(a)). A thin intermediate phase layer approximately 1 μm thick was observed in successful joints. Several grains were also observed in this layer which exhibited similar contrast to the secondary particles that originally existed within the AA2024 aluminum stud.

3.2. Intermediate phase layer

Joint interfaces were observed in more detail by using an FE-SEM to investigate the thin intermediate phase layer more clearly. Fig. 16 shows an FE-SEM-BEI micrograph of the joint interface formed under a discharge voltage of 300 V. Two distinct thin intermediate phase layers exhibiting different contrasts are clearly visible. The different layers are marked by points (a) and (b) in Fig. 16, respectively. Several grains were also observed in the intermediate phase layer (point (c)), as can also be seen in Figs. 11(c) and 15(b). Fig. 17 shows Auger spectra of points (a)–(c) from Fig. 16. The relative sensitivity factor method was employed in the quantitative analysis by AES. Chemical compositions of points (a)–(c) are listed in Table 3. Minoda and Yoshida (2010) reported that Al_2CuMg was observed in homogenized AA2024 aluminum. Several grains observed in the intermediate phase layer (point (c)) were estimated to be intermetallics of the Al–Cu–Mg system (Al_2CuMg), which had originally existed within the AA2024 aluminum stud. According to the Al–Mg binary phase diagram (Massalski et al., 1986) and Table 3, the intermediate phase layers (points (a) and (b)) were

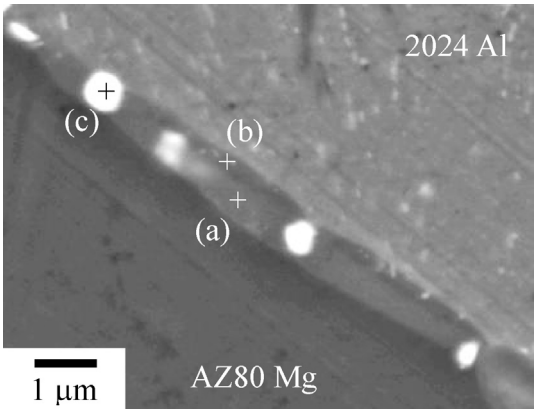

Fig. 16. FE-SEM-BEI micrograph of joint interface formed under discharge voltage of 300 V.

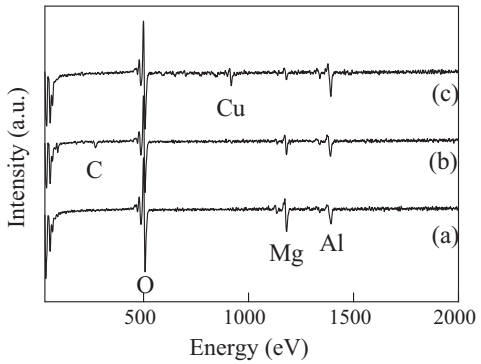

Fig. 17. Auger spectra of points (a)–(c) in Fig. 16.

Table 3
Chemical compositions of points (a)–(c) in Fig. 16, atom%.

	Al	Mg	Cu	Compound
(a)	45.4	54.6	–	$Mg_{17}Al_{12}$
(b)	62.9	37.1	–	Al_3Mg_2
(c)	68.3	12.5	19.2	Al_2CuMg

confirmed to be $Mg_{17}Al_{12}$ and Al_3Mg_2; the thickness of each layer was about 500 and 300 nm, respectively. Liu et al. (2004) reported the formation and growth of intermediate phases in Al–Mg diffusion coupled with an electromagnetic field. The diffusion zone was composed of two intermediate phases ($Mg_{17}Al_{12}$ and Al_3Mg_2). Bu et al. (2011) deposited aluminum coatings on AZ91D magnesium substrates using the cold spray process. It was found that $Mg_{17}Al_{12}$ and Al_3Mg_2 intermetallics are formed at the coating/substrate interface during subsequent heat treatment at 400 °C. Yamamoto et al. (2009) also reported that intermetallic compound layers consisting of $Mg_{17}Al_{12}$ and Al_3Mg_2 are formed at the bonding interface of dissimilar friction stir welded joints, and that the formation and growth of the intermetallic compounds is controlled by the diffusion of Mg and Al atoms, instead of the eutectic reaction. The Al_3Mg_2 layer was thicker than the $Mg_{17}Al_{12}$ layer in their studies, which is the reverse of the present results. Shigematsu et al. (2000) reported the formation process of a reacted layer between magnesium plate and aluminum particles. First, diffusion occurs at the points of contact between magnesium and aluminum. Intermetallic compounds having a low melting point (approximately 450 °C) then form at the contact points. These begin melting as the temperature rises above the melting point, and diffusion accelerates through the liquid phase. Yamamoto et al. (2009) also suggested that more $Mg_{17}Al_{12}$ phase will form if the intermetallic compound layer forms due to a eutectic reaction at higher temperature, since the eutectic temperature of Mg and $Mg_{17}Al_{12}$ (437 °C) is lower than that of Al and Al_3Mg_2 (450 °C). Thus, in the present study, the interfacial temperature for forming sound joints was considered to be above such eutectic temperatures. Yamamoto et al. (2009) reported that the tensile strength of friction stir welded joints decreases considerably when the thickness of the intermetallic compound layer is >1.8 μm. Since the intermediate phase layers observed in the present study were very thin (<1 μm, in total) as a result of suppressing excess heat input for joining, sufficient joining between an aluminum alloy stud and magnesium alloy plate was achieved by high-speed solid-state welding.

4. Conclusions

A high-strength AA2024-T3 aluminum stud were successfully joined to AZ80-F magnesium extruded plate by a high-speed solid-state welding. Discharge voltages for joining were set at 250–400 V. The following results were obtained.

(1) Maximum tensile fracture load was achieved in specimens joined under a discharge voltage of 300 V. Appropriate selection of the discharge voltage was important for sound joining.
(2) The joining behavior was different from that observed in a previously reported joining of AA2024 aluminum studs to AA5052 aluminum plate and to AA6N01 aluminum plate.
(3) Refined grains of AZ80 magnesium were observed near the joint interface. This reveals that local plastic deformation and heating induced dynamic recrystallization within the plate.
(4) A thin layer of $Mg_{17}Al_{12}$ and Al_3Mg_2 approximately 1 μm in thickness was observed along the joint interface. Optimal temperature around the projection was found to contribute to forming sound joints, with a thin intermediate phase layer forming along the joint interface.

Acknowledgements

The authors thank Mr. Kenji Kitayama, Dr. Tsunenari Saito, and Mr. Yoshinori Kubodera of Akebono Kikai Ltd. for technical support and useful discussion. The authors also thank Dr. Masaru Tada (Center for Advanced Materials Analysis, Tokyo Institute of Technology) for technical support in AES observations.

References

Bu, H., Yandouzi, M., Lu, C., Jodoin, B., 2011. Effect of heat treatment on the intermetallic layer of cold sprayed aluminum coatings on magnesium alloy. Surface and Coatings Technology 205, 4665–4671.
Bhamji, I., Preuss, M., Moat, R.J., Threadgill, P.L., Addison, A.C., 2012. Linear friction welding of aluminum to magnesium. Science and Technology of Welding and Joining 17 (5), 368–374.
Chambers, H.A., 2001. Principle and practices of stud welding. PCI Journal 46 (5), 46–58.
Firouzdor, V., Kou, S., 2010. Al-to-Mg friction stir welding: effect of material position, travel speed, and rotation speed. Metallurgical and Materials Transactions A 41, 2914–2935.
Kumai, S., Hayashida, K., Watanabe, M., 2011. Advanced high-speed solid-state joining of 2024 aluminum alloy studs to 5052 aluminum alloy plates. Materials Transactions 52 (5), 992–998.
Kumai, S., Takaya, K., 2012. Effects of plate thickness on microstructure and strength of high-speed solid-state joined 2024 aluminum alloy stud and 5052 aluminum alloy plate. Journal of Japan Institute of Light Metals 62 (8), 293–299.
Kumai, S., Hayashida, K., 2012. Projection shape modification for improvement in joining strength of high-speed solid-state joined 2024 aluminum alloy stud and 5052 aluminum alloy thin plate. Journal of Japan Institute of Light Metals 62 (9), 331–337.
Liu, X., Cui, J., Guo, Y., Wu, X., Zhang, J., 2004. Phase formation and growth in Al–Mg couple with an electromagnetic field. Materials Letters 58, 1520–1523.
Massalski, T.B., Murray, J.L., Bennett, L.H., Baker, H., 1986. Binary Alloy Phase Diagrams, vol. 1. American Society for Metals, Metals Park, OH, pp. 129–131.
Minoda, T., Yoshida, H., 2010. Influence of solute atoms on thermal stability of fibrous structure in 2024 aluminum alloy extrusion. Journal of Japan Institute of Light Metals 60 (9), 451–457.
Ramasamy, S., 2002. Drawn arc aluminum stud welding for automotive applications. Journal of the Minerals, Metals and Materials Society 54 (8), 44–46.
Schubert, E., Klassen, M., Zerner, I., Walz, C., Sepold, G., 2001. Light-weight structures produced by laser beam joining for future applications in automobile and aerospace industry. Journal of Materials Processing Technology 115, 2–8.
Shigematsu, I., Nakamura, M., Saitou, N., Shimojima, K., 2000. Surface treatment of AZ91D magnesium alloy by aluminum diffusion coating. Journal of Materials Science Letters 19, 473–475.
Takaya, K., Harada, Y., Kumai, S., Kitayama, K., 2012. Microstructure of joint interface and mechanical properties in high-speed solid-state welded 2024 aluminum alloy stud and 6N01 aluminum alloy plate. Journal of Japan Institute of Light Metals 62 (10), 370–376.
Watanabe, T., Sugiyama, Y., 2004. Resistance spot welding of a magnesium alloy AZ31B plate to a 1050 aluminum plate using Ag insert metal. Journal of Japan Institute of Light Metals 54 (7), 293–297.
Yamamoto, N., Liao, J., Watanabe, S., Nakata, K., 2009. Effect of intermetallic compound layer on tensile strength of dissimilar friction-stir weld of a high strength Mg alloy and Al alloy. Materials Transactions 50 (12), 2833–2838.